

LPM effect and dielectric suppression in air showers

A. N. Cillis, H. Fanchiotti, C. A. García Canal and S. J. Sciutto

*Laboratorio de Física Teórica
Departamento de Física
Universidad Nacional de La Plata
C. C. 67 - 1900 La Plata
Argentina
e-mail: cillis@venus.fisica.unlp.edu.ar*

31st January 2019

Abstract

An analysis of the influence of the Landau-Migdal-Pomeranchuk (LPM) effect on the development of air showers initiated by astroparticles, is presented. By means of computer simulations using algorithms that emulate Migdal's theory, including also the so-called dielectric suppression, we study the behaviour of the relevant observables in the case of ultra high energy primaries. We find that the LPM effect can significantly modify the development of high energy electromagnetic showers.

1 Introduction

There are some effects that drastically reduce the cross sections of electron bremsstrahlung and pair production [1] of atmospheric air showers initiated by high energy astroparticles. These suppression mechanisms can affect air showers by lengthening the showers, and consequently moving the position of the shower maximum deeper into the atmosphere. Two suppression mechanisms have been studied in the present work, namely, the Landau-Pomeranchuk-Migdal (LPM) effect [2, 3] due to the multiple scattering and the dielectric suppression [1] due to the interaction of the bremsstrahlung photons with the atomic electrons in the medium through forward Compton scattering.

By means of numerical simulations we have studied the influence of these effects on the development of air showers. We have used the AIRES program to perform such simulations. AIRES [4] represents a set of programs to simulate atmospheric air showers and to manage all the associated output data. The physical algorithms of the AIRES system are based on the realistic procedures of the well-known MOCCA program [5]. AIRES provides some additional features, for example: The Earth's curvature is taken into account allowing safe operation of all zenith angles; the simulation programs can be linked to several alternative hadronic collision models; etc. To complete our study we have incorporated new LPM and dielectric suppression algorithms to the AIRES code.

2 Migdal theory

The LPM effect was first predicted by Landau and Pomeranchuk some 40 years ago. Migdal [3] provided the corresponding quantum mechanical theory giving analytical expressions for the bremsstrahlung and pair production cross sections. Recently an experiment performed at SLAC [6] using targets of different compositions, measured the LPM effect founding that there is acceptable agreement between the experimental data and the Migdal's theory that is presently considered the standard treatment.

Let us consider first the case of bremsstrahlung where an electron or positron of energy E emits a photon of energy k in the vicinity of a nucleus of charge Z . The Migdal cross section for this process is ($c = 1$, $\hbar = 1$) [3]:

$$\frac{d\sigma_{LPM}}{dk} = \frac{4\alpha r_e^2 \xi(s)}{3k} \{y^2 G(s) + 2[1 + (1 - y)^2] \phi(s)\} Z^2 \ln \left(\frac{184}{Z^{\frac{1}{3}}} \right) \quad (1)$$

where

$$y = \frac{k}{E}, \quad (2)$$

$$s = \sqrt{\frac{E_{LPM} k}{8E(E - k)\xi(s)}}, \quad (3)$$

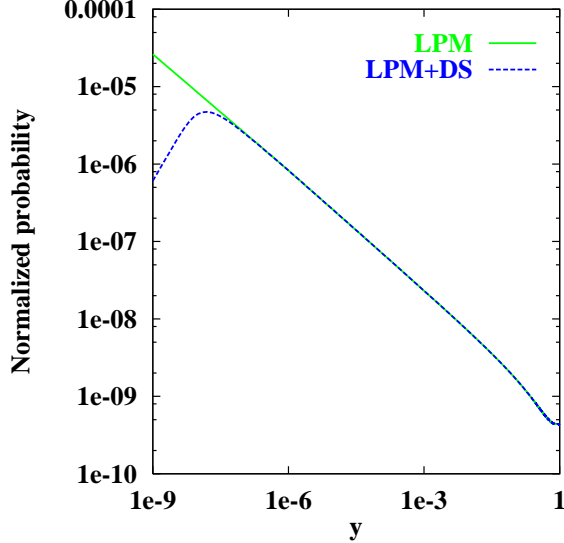


Figure 1.

Bremsstrahlung normalized probability versus photon energy, as given by Migdal's theory, with and without dielectric suppression. The electron energy is 10^{18} eV and the medium is air (atmospheric depth 1000 g/cm²).

$$G(s) = 48s^2 \left(\frac{\pi}{4} - \frac{1}{2} \int_0^\infty e^{-st} \frac{\sin(st)}{\sinh(t/2)} dt \right), \quad (4)$$

$$\phi(s) = 12s^2 \left(\int_0^\infty e^{-st} \coth(t/2) \sin(st) dt \right) - 6\pi s^2, \quad (5)$$

$$\xi(s) = \begin{cases} 2 & \text{if } s < s_1 \\ 1 + \ln(s)/\ln(s_1) & \text{if } s_1 \leq s \leq 1 \\ 1 & \text{if } s > 1 \end{cases} \quad (6)$$

($s_1 = Z^{2/3}/184^2$). r_e is the classical electron radius ($r_e = e^2/m$). E_{LPM} is the characteristic energy of the LPM effect and is given by

$$E_{LPM} = \frac{m^4 X_0}{E_s^2}. \quad (7)$$

X_0 is the radiation length and

$$E_s = m\sqrt{4\pi/\alpha} = 21.2 \text{ MeV}. \quad (8)$$

To measure the strength of the effect it is convenient to introduce the suppression factor through

$$S = \frac{d\sigma_{LPM}/dk}{d\sigma_{BH}/dk} \quad (9)$$

where $d\sigma_{BH}/dk$ stands for the ‘‘classical’’ bremsstrahlung cross section given by the theory of Bethe and Heitler [7].

The strength of the effect largely depends on the variable s of equation (3). For $s \ll 1$, the suppression is important ($S \ll 1$), while for $s \gg 1$, there is no suppression ($S \cong 1$). In fact, when $s \rightarrow \infty$, the Migdal cross section reproduces, up to 3 %, the

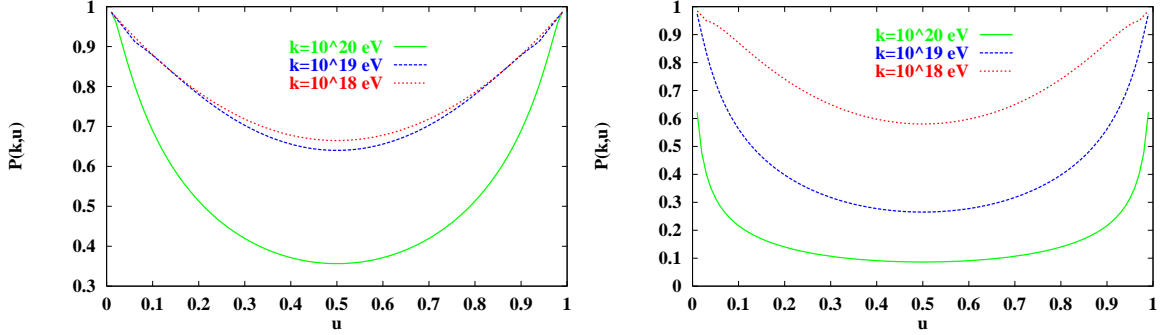


Figure 2. Migdal formulation: Pair production. *a)* $P(k,u)$, $X = 50g/cm^2$. *b)* $P(k,u)$, $X = 1000g/cm^2$.

main terms of the Bethe-Heitler equation [1, 7].

The characteristic energy E_{LPM} gives the energy scale where the effect is significant. Notice that E_{LPM} diminishes when the density of the medium is enlarged. Therefore, for dilute media the LPM effect will be appreciable only for very high energies. For air in normal conditions, for example, taking $Z = 7.3$, $\rho = 1.2 \text{ Kg}/\text{m}^3$ we have $E_{LPM} = 223 \text{ PeV}$.

On the other hand, when $k \rightarrow 0$, it is necessary to take into account the change of the photon momentum due the fact that the dielectric constant of the medium is different from one. By considering $k \gg \omega_p$ one obtains: $\varepsilon = 1 - \omega_p^2/k^2$, where ω_p is the well-known plasma frequency (for air $\hbar\omega_p = 0.73 \text{ eV}$). The Migdal approach takes into account this effect usually called dielectric suppression. The influence of the dielectric suppression on the bresstrahlung cross section is well noted in Figure 1 where the normalized probability for bresstrahlung is plotted against y in the case of $E = 10^{18} \text{ eV}$. Notice how the emission probability is suppressed for $y < 10^{-8}$. Since the energy $E = 10^{18} \text{ eV}$ this corresponds to photon energies $k < 0.01 \text{ TeV}$.

We go now into the pair production processes. In this case the cross section coming from Migdal's theory reads

$$\frac{d\sigma_{LPM}(\gamma \rightarrow e^+e^-)}{dE} = \frac{4\alpha r_e^2 \xi(\tilde{s})}{3k} \{G(\tilde{s}) + 2[u + (1-u)^2]\phi(\tilde{s})\} Z^2 \ln\left(\frac{184}{Z^{1/3}}\right) \quad (10)$$

where

$$u = \frac{E}{k} \quad (11)$$

and

$$\tilde{s} = \sqrt{\frac{E_{LPM}k}{8E(k-E)\xi(\tilde{s})}} \quad (12)$$

Figure 2 shows the normalized probability of pair production at atmospheric depth of 50 and 1000 g/cm² and for different energies of the primary photon. Notice how the production probabilities are progressively suppressed when the primary energy rises. From the figure above, it is also evident that symmetric processes are more affected by the suppression mentioned.

3 Practical Implementation

The AIRES simulation system [4] has been used as a realistic program to perform the simulations needed to make our analysis. The LPM effect and the dielectric suppression have been incorporated into the AIRES program.

When the characteristics of the atmosphere are taken into account it comes out that the LPM effect must be considered for all the events where the energy of the primary is larger than 100 TeV. This ensures that the effective cross sections are calculated with a relative error that is never larger than a few percent.

4 Simulations

We have analyzed the influence of the LPM effect and the dielectric suppression on the air shower development, performing simulations for different primary energies (from 10¹⁴ to 10²¹ eV) and different primary particles initiating the showers (gamma, proton, electron).

For showers initiated by gammas with primary energy larger than 10²⁰ the impact of the LPM effect is evident. It affects the position of X_{\max} (the maximum of the shower), the number of particles at X_{\max} and the fluctuations of these magnitudes. This is shown in Figure 3, where the total number of charged particles is plotted against the vertical depth (longitudinal development of all charged particles) for two different primary energies. The LPM effect affects the gamma showers lengthening and consequently moving the average position of X_{\max} deeper into the atmosphere. This effect is evident in Figure 4.a where one sees that X_{\max} is shifted in approximately 100 g/cm² for 10²⁰ eV and 500 g/cm² for 10²¹ eV. The fluctuations of X_{\max} also increase when the LPM effect is taken into account as can be seen in Figure 4.b. The average number of charged particles at X_{\max} is reduced and its fluctuations are larger when the LPM effect is introduced as can be seen in Figure 5 for gamma showers of more than 10²⁰ eV. We have not found appreciable differences for gamma initiated showers with primary energies less than 10¹⁸ eV. This allow us to conclude that even if the LPM effect must be taken into account for all particles with energies larger than 100 TeV, the fraction of such events is statistically significant only for electromagnetic showers initiated by primaries with energies larger than 10¹⁸ eV.

In Figure 6 the total number of μ^\pm is plotted against the vertical depth (longitudinal development of μ^\pm) against two different energies. This observable is very important in the determination of the primary composition. In agreement with the longitudinal development of all charged particles, it presents the same modifications when the LPM effect is taken into account.

For air showers initiated by protons, no measurable differences appear neither in the average X_{\max} , nor in the fluctuations of this quantity. The protons interact hadronically, and then, the electromagnetic shower, where the LPM effect takes place, starts later. The proton primary energy is shared among the secondary showers after the first interaction and the electromagnetic cascade begins with energies that are about 2-4 orders of magnitude less than the initial proton energy. Therefore, one should compare the 10^{20} proton showers with the gamma showers of initial energies of 10^{17} - 10^{18} eV, where we have not found appreciable differences between showers with and without LPM effect. The longitudinal development of all charged particles for proton initiated showers is plotted in Figure 7. The differences between the simulations with and without dielectric suppression are less important and are shown in Figure 3 and 6 for the showers initiated by gammas.

Finally notice that the characteristics of electron initiated showers are very similar to those corresponding to gamma showers and for this reason we have not included here any related plots.

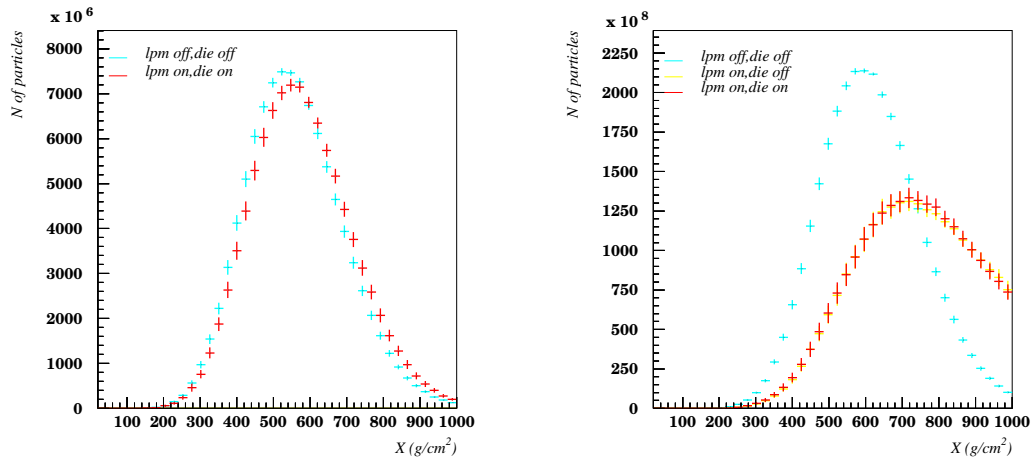


Figure 3. Longitudinal development: All charged particles. Parameters: Primary particle: γ . Primary energy: 10^{19} eV, 3×10^{20} eV. Zenith 60° . Thinning energy: 10^{-5} rel. Injection altitude: 100 km.

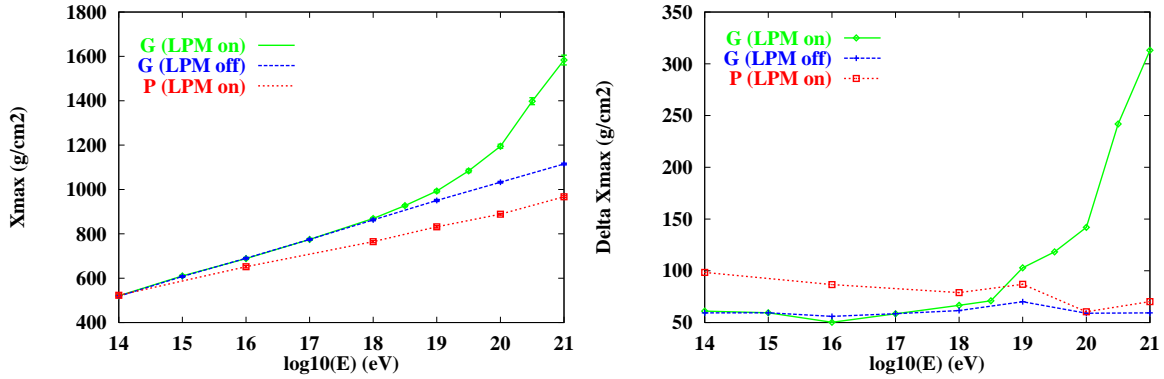


Figure 4. Shower maximum X_{max} (a), and X_{max} fluctuations (b) for gamma and proton showers.

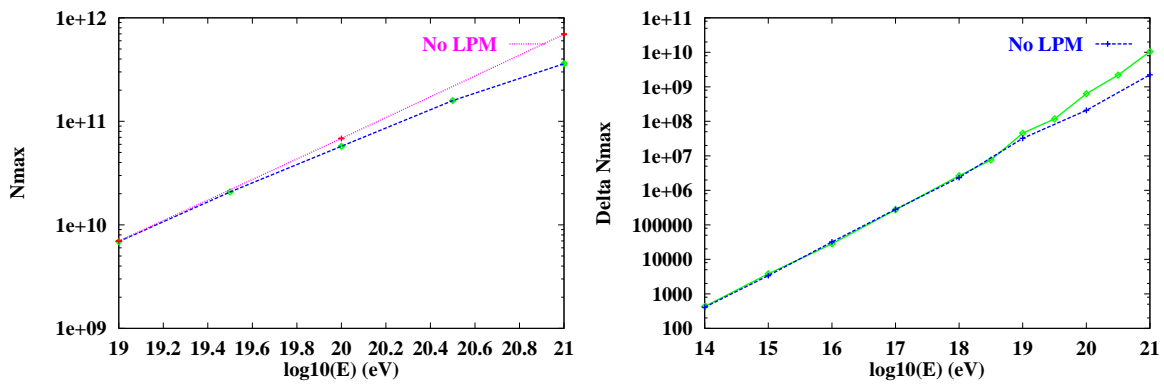


Figure 5. Number of charged particles at X_{max} , N_{max} (a), and N_{max} fluctuations (b) for gamma showers.

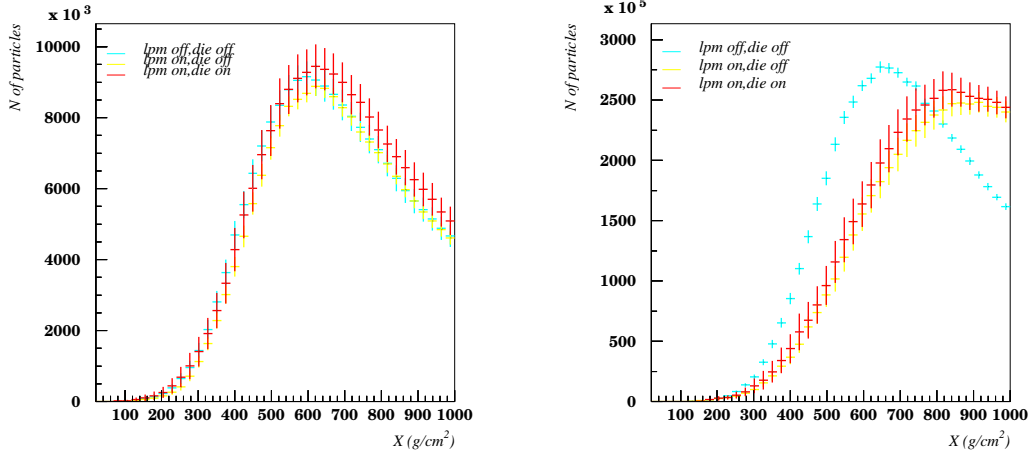


Figure 6. Longitudinal development of muons. Parameters: Primary particle: γ . Primary energy: 10^{19} eV, 3×10^{20} eV. Zenith 60° . Thinning energy: 10^{-5} rel. Injection altitude: 100 km.

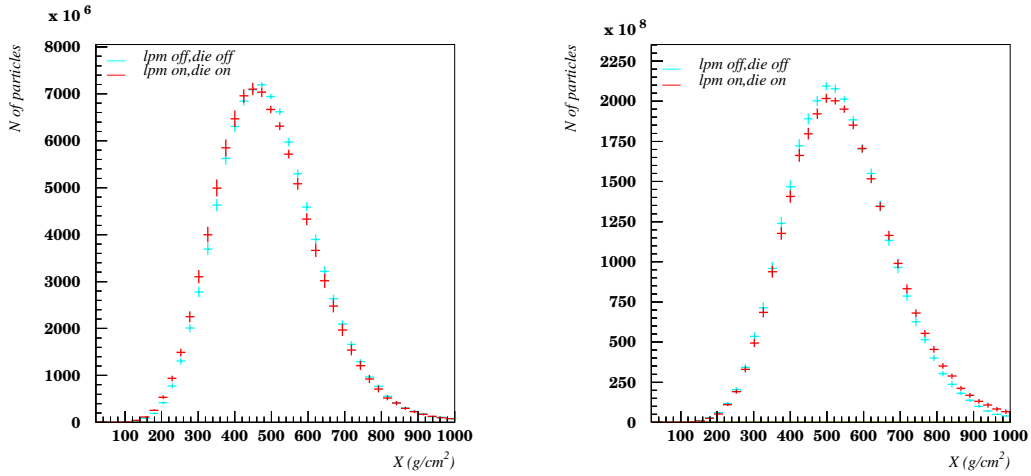


Figure 7. Longitudinal development: All charged particles. Parameters: Primary particle: p . Primary energy: 10^{19} eV, 3×10^{20} eV. Zenith 60° . Thinning energy: 10^{-5} rel. Injection altitude: 100 km.

5 Conclusions

The LPM effect introduces modifications on the development of gamma and electron air showers if the primary energies are larger than 10^{19} eV. These effects can be observed in the longitudinal development of the showers. The X_{\max} position for such initial conditions moves deeper into the atmosphere and its fluctuations are increased when the LPM effect is taken into account. The longitudinal development of μ^\pm also changes in concordance with all charged particles case.

We have not found any significant effect if the showers are initiated by proton with primary energies up to 10^{21} eV, because in this case, the electromagnetic shower, where the LPM effect takes place, begins later, when the initial energy is shared among the secondary particles, reducing the initial proton energy in 2-4 orders of magnitude. Clearly the same reasoning is valid for nuclei primary cosmic rays.

References

- [1] S. Klein, *hep-ph/9802442* (1998).
- [2] L.D. Landau and I.J. Pomeranchuk , *Dokl. Akad. Nauk SSSR*, **92**, 535 (1953); *Dokl. Akad. Nauk SSSR*, **92**, 735. These papers are available in English in *The Collected Papers of L. D. Landau*, Pergamon Press, 1965.
- [3] A.B. Migdal, *Phys. Rev.* **103**, 1811 (1956).
- [4] S. J. Sciutto, *AIRES, a system for air shower simulations. User's manual and reference guide*, Pierre Auger Observatory technical note GAP-98-032 (1998).
- [5] A. M. Hillas, *Proc. 19th ICRC (La Jolla)*, **1** , 155 (1985).
- [6] Anthony, P et al., *Bremsstrahlung suppression due to LPM and dielectric effects in a variety of targets*, *Phys.Rev.* **D56**, 1373 (1997).
- [7] H.A. Bethe and Heitler, *Proc. Royal Soc.* **A 146**, 83 (1934).